Vietnam Journal of Catalysis and Adsorption
Tạp chí xúc tác và hấp phụ Việt Nam

https://jca.edu.vn

Manganese oxide derived from spent primary batteries as anode material for lithium-ion batteries

Le Thi Thanh Lieu[1,*], Ho Doan Phuong Thao[2], Nguyen Ngoc Dieu[2], Lam Thi Thuy Kieu[2], Nguyen Tu Quyen[2], To Thy Thuong[1], Tran Thi Truc Quynh[2], Vien Vo[1]

[1] *Faculty of Natural Sciences, Quy Nhon University, 170 An Duong Vuong, Quy Nhon, Binh Dinh*
[2] *Faculty of Education, Quy Nhon University, 170 An Duong Vuong, Quy Nhon, Binh Dinh*
** Email: lethithanhlieu@qnu.edu.vn*

ARTICLE INFO

Received: 25/02/2024
Accepted: 18/07/2024
Published: 30/12/2024

Keywords:
Manganese oxide;
spent primary batteries;
recycling;
lithium-ion batteries anode

ABSTRACT

The unstoppably increasing demand for renewable energy concomitates the rapid increase in production and the disposal of spent energy storage systems, including primary batteries, which has caused a serious impact on the environment. The feasible and facile procedure for recycling the spent primary batteries could not only reduce this dangerous waste but also provide an economical strategy for sustainable development. This work has applied a facile thermal treatment to recover the manganese oxide from the wasted alkaline batteries from the local market. The obtained materials were used as anode for lithium-ion batteries in a half-cell configuration. The galvanostatic results of the recycled electrodes performed a specific discharge capacity of 102 mAh g^{-1} after 50 cycles and a good rate capacity of 208 mAh g^{-1} at a specific current of 1000 mA g^{-1}. These results suggest the potential of research in the future industrial recycling aspect.

Introduction

Primary batteries, particularly alkaline and Zn-C batteries, are widely used in various modern devices in our daily lives, including radios, watches, toys, lights, cameras, remote controls, alarm clocks, and phones. However, due to their short lifespan and one-time use, many spent primary battery cells are generated yearly [1]. Alkaline and Zn-C batteries contain valuable elements like Zn, Mn, C, Cu, Fe, etc., which must be recovered to support a circular economy. The recovery of Zn and Mn from waste batteries is crucial in the recycling process [2]. Two common routes for recovering Mn and Zn from spent alkaline and Zn-C batteries are pyrometallurgical and hydrometallurgical processes [1-3]. While the hydrometallurgical treatment involves the use of complex solvents, is costly, and requires a relatively large amount of chemicals for metal recovery, pyrometallurgical techniques are commonly used to recover metals from waste primary batteries with the advantages of a high rate of chemical reactions, large treatment capacity, and simple operation. Nevertheless, the pyrometallurgical process is typically carried out to recover spent batteries at 900 °C [4], 950 °C [5], 1150 °C [6], and 1200 °C [7].

Lithium-ion battery (LIB) technology is crucial for our modern lifestyle in terms of energy storage *and* reliable energy sources for electric vehicles. Recently, transition metal oxides have shown higher specific capacities (over 800 $mAhg^{-1}$) than graphite (372 $mAhg^{-1}$) and are replacing commercial graphite anodes. Among reported transition metal oxides, Mn_3O_4 is favored by researchers due to its low cost, environmental friendliness, and low working potential [8].

https://doi.org/10.62239/jca.2024.066

The main objective of this paper is to propose a simple thermal transformation at 550 ˚C under air for treating black mass from spent primary batteries to synthesize Mn_3O_4 materials, which exhibit good electrochemical performance as electrodes in lithium storage. The novelty of the current work is the facile thermal treatment under air at lower temperatures, which offers environmental advantages such as lower gas emissions and reduced energy consumption compared to previously reported processes [4-7].

Experimental

Chemicals

Hydrochloric acid (HCl) (35-37%) is from Xilong, China, and is used without further purification. Polyvinylidene fluoride (PVDF) (Mw 534000, Sigma Aldrich), 1-methyl-2-pyrrolidione (NMP, 99.5%, Sigma Aldrich), and black mass were collected from Spent primary batteries AA Panasonic 1.5 V.

Synthesis of Mn_3O_4

Spent primary batteries (AA Panasonic 1.5 V) were dismantled manually to separate the black mass from components of the battery, such as zinc casing, carbon rod, separator, and sealing. The obtained battery black mass was dried in the oven at 80 °C for two hours to remove moisture, denoted by BM. An amount of black mass (2 g) was placed in a ceramic crucible and heated to 550 ºC for four hours under an air atmosphere with a heating rate of 10°C·min^{-1}. Obtained powder after thermal transformation was washed with HCl 5%, then washed several times with distilled water and ethanol, before being dried in an oven at 80 °C for 12 h to synthesize Mn_3O_4 nanoparticles, which were characterized and used as an active material for LIB anode.

Materials characterization

The surface morphology of the synthesized materials was characterized by scanning electron microscopy (SEM) using a HITACHI S-4800 microscope. The crystalline structure of the samples was studied by powder XRD using a Bruker D2 Advance diffractometer equipped with a Cu-Kα X-ray source (λ = 0.154 nm. The spectra were acquired in the 2θ range of 10 – 70°. The Fourier-transform infrared (FT-IR) spectroscopy was carried out on FTTR-affinity-1S, Shimadzu spectrophotometer, ratio S/N: 30000:1 with a sample concentration of 1% in weight in KBr pellet.

For electrochemical measurements, the materials (BM, Mn_3O_4) were well-mixed with Super P Conductive Carbon and PVDF as binder with a mass ratio of 75:15:15 in solvent to generate a homogeneous slurry. Subsequently, the slurry was cast onto a copper foil, dried in a vacuum oven at 120 °C for 24 h, and punched to produce disc-shape working electrodes with a diameter of 10 mm. These discs were used as working electrodes and assembled into CR2032-type coin cells that used a lithium foil as the counter and reference electrode and a glass fiber pad as the separator. The separator pad was soaked into 180 µL of 1 M LiPF6 solution of a solvent mixture of dimethyl carbonate (DMC) and ethylene carbonate (EC) (1:1 by volume).

LAND-CT2001A battery workstations were used to perform the galvanostatic cycling with potential limitation (GCPL) tests with a voltage range of 0.1–3.0 V (*vs.* Li/Li$^+$) at a specific current of 100 mA·g^{-1} for the initial five cycles and 1000 mAh·g^{-1} for the following cycles. The rate performance was conducted in the same condition with various specific currents from 100 to 5000 mA·g^{-1}. A Biologic-MPG2 electrochemical workstation was used to take Cyclic voltammetry (CV) tests at a scan rate of 0.1 mV·s^{-1}, and Electrochemical impedance spectroscopy (EIS) tests were recorded at the assembled cells' open circuit voltage (OCV) after six hours of resting on a Biologic VSP3 potentiostat. The frequency range and AC perturbation were set to 100 kHz ~ 10 mHz and 10 mV, respectively.

Results and discussion

SEM images observe material morphology, and the corresponding EDS spectra are shown in Fig. 1a-d. In Figure 1a, the spherical BM nanoparticles are aggregated with a wide range of particle sizes, while according to Figure 1b, the Mn_3O_4 nanoparticles are well-dispersed.

The EDS spectra (Fig. 1c, d) and Table 1 reveal that the surface elements of both MB and Mn_3O_4 materials comprise zinc, manganese, carbon, oxygen, aluminum, silicon, and chlorine. However, compared to BM, the main transition components of the Mn_3O_4 sample were carbon and zinc after thermal treatment and being washed with HCl 5% solution. Consequently, for the Mn_3O_4 material, the significant elements are manganese and oxygen, whereas minor elements like carbon and other trace elements like zinc, aluminum, silicon, and chlorine are also present.

XRD patterns of the BM (Fig. 1e) and synthesized Mn_3O_4 powder (Fig. 2e) assigned to an amorphous material and a tetragonal Mn_3O_4 (Hausmannite) phase (ICDD Code: 04-006-8183), respectively. The diffraction peak positions at 2θ = 18, 29, 31, 32, 36, 38, 44, 51, 59, 60, and 65° were corresponded to crystal planes of (101), (112), (200), (103), (211), (004), (220), (105), (321), (224) and (400) of Mn_3O_4, respectively [8],

The BM and Mn_3O_4 were analyzed by FTIR spectroscopy from 4000 to 400 cm^{-1}. The spectrum (Fig. 1f) shows the characteristic absorption bands of υMn–O vibrations at 608, 489, and 410 cm^{-1}, together with a strong band at 1046 cm^{-1}, which can be attributed to υMn–O–H vibration. Additionally, the absorption peak around 1621, 1552, and 1394 cm^{-1} could be attributed to O-H bending vibration combined with Mn atoms [9]. The FTIR band at ~ 3451 cm^{-1} is attributed to the stretching vibration of OH groups in the battery black mass. In addition, the band at 805 cm^{-1} corresponds to the stretching vibration modes of Zn-Cl units [4], which is not observed for Mn_3O_4. The FTIR bands at ~608, 489, and 410 cm^{-1} are characteristic of Mn-O bonding and attributed to the stretching vibration of the spinel metal oxide of $MnO.Mn_2O_3$ [10, 11].

Table 1. Characterization of black mas from spent alkaline Panasonic AA 1.5V battery powders by EDS.

	BM		Mn_3O_4	
Element	Weight %	Atomic %	Weight %	Atomic%
C K	33.13	57.21	10.52	21.75
O K	18.72	24.27	31.21	50.51
Al K	0.20	0.16	0.15	0.15
Si K	0.65	0.48	0.42	0.39
Cl K	6.17	3.61	0.36	0.27
Mn K	20.21	7.63	56.35	26.56
Zn K	20.91	6.63	0.94	0.37

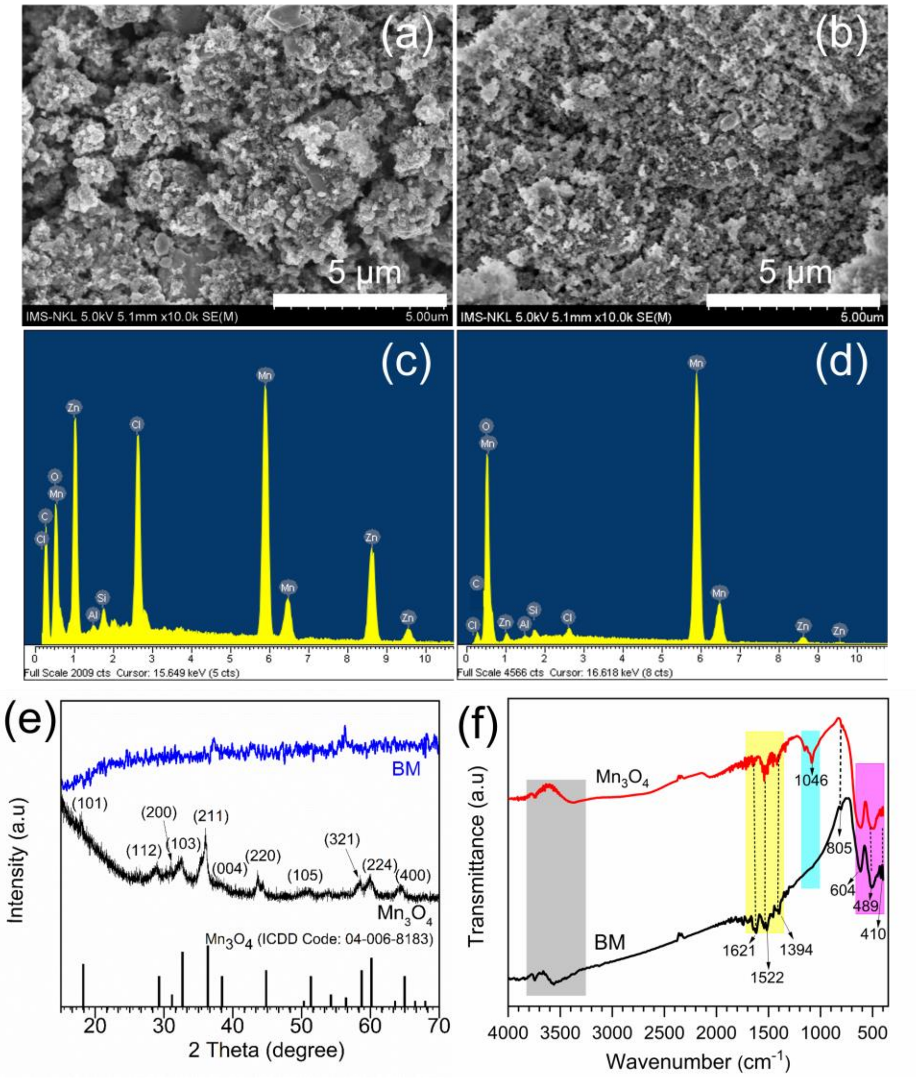

Fig. 1: SEM images of BM (a), Mn_3O_4 (b); EDS spectra of BM (c) and Mn_3O_4 (d); XRD patterns (e), and IR spectra (f) of BM and Mn_3O_4

https://doi.org/10.62239/jca.2024.066

The electrochemical behavior of lithiation/delithiation over BM and Mn_3O_4 electrodes was investigated using CV curves electrodes by scanning the potential from 3 V to 0.01 V (versus Li/Li^+) at a scan rate of 0.1 mV s^{-1}. Figure 2 (a, b) illustrates the CV test results. For the Mn_3O_4 anode (Fig. 2b), the first cathodic cycle shows the sharp peak observed at a lower potential of 0.1 V can be assigned to the reduction of Mn_3O_4 to metallic manganese (eq. 1) [12].

$$Mn_3O_4 + 8Li^+ + 8e \longleftrightarrow 3Mn + 4Li_2O \quad (1)$$

After the first cycle, cathodic peaks shift to a higher potential of 0.28 V (2nd cycle) and 0.34 V (3rd cycle) due to improved kinetics after lithiation [12]. The anodic peak observed around 1.23 V corresponds to the reoxidation of metallic manganese to Mn_3O_4 [12], The GCPL profiles of two electrodes in the first three cycles are shown in Figure 2c, d, within the voltage range of 0.1–3.0 V (versus Li/Li^+) at a specific current of 100 mA·g^{-1}. For the first discharge curve of Mn_3O_4, a 0.3 V discharge plateau was observed, and the gentle slope to 0.1 V is primarily attributed to Mn_3O_4 reduction. In addition, one apparent slope is also found in the first charge profile at 1.0−1.6 V, reflecting measurements of Mn to Mn_3O_4 oxidation conversion, respectively. However, in the following scans, the voltage-capacity curves changed, indicating a poor cycling performance of Mn_3O_4, which was also observed in reported publications [13-17].

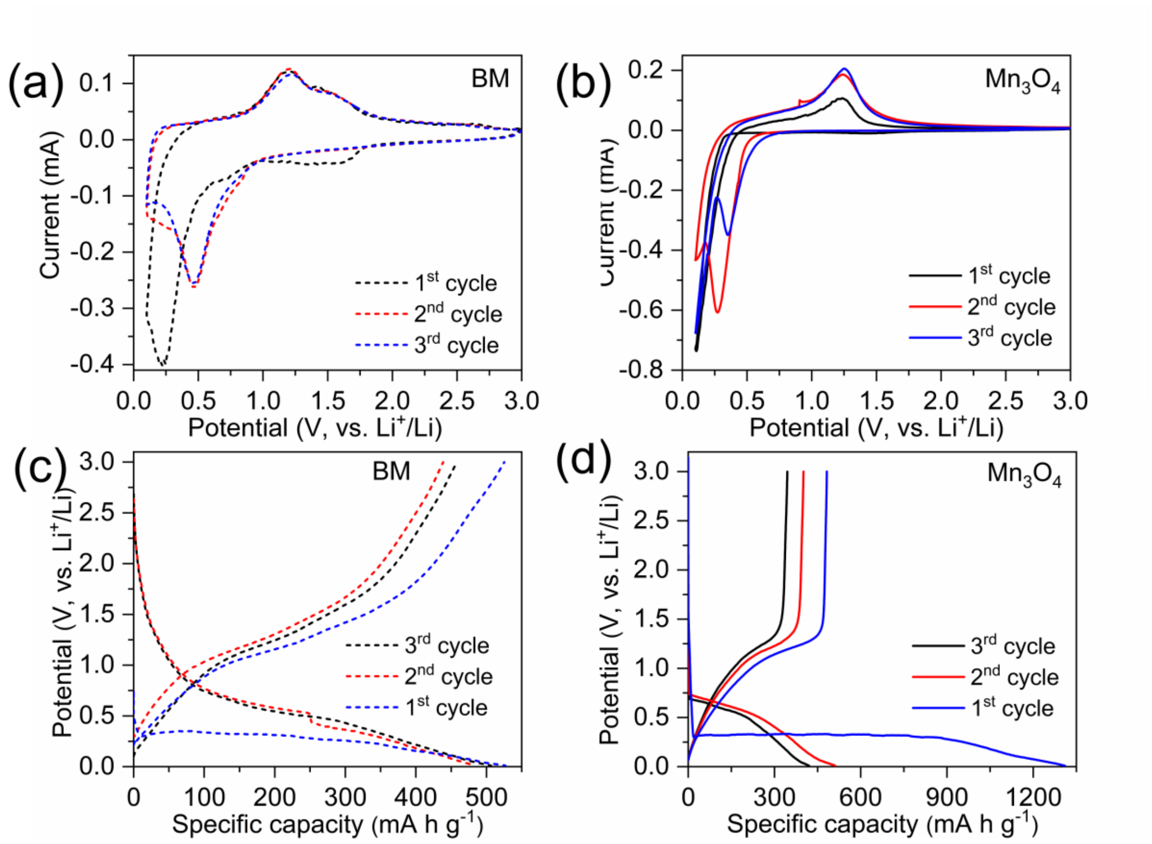

Fig. 2: (a, b)- CV results and (c, d)- GCPL profiles for the three first cycles of BM and Mn_3O_4 electrodes

Furthermore, all electrodes' Nyquist plots (Figure 3a) comprise a semicircle in the high-to-medium frequency range, including two components: the diameter of the semicircle is related to charge transfer resistance at the electrode-electrolyte interface, while the latter tail presents the diffusion of ions in the solid phase. Mn_3O_4 possesses the smaller diameter of the semicircle, followed by BM, indicating that Mn_3O_4 has a lower contact resistance and a greater charge transfer rate at the electrode-electrolyte interface.

An additional examination of the consecutive cycling behavior at different charge-discharge rates, measured after 30 cycles in ascending steps from 100 to 5000 mA g^{-1}, is presented in Figure. 3b. The Mn_3O_4 electrode delivers specific capacities of 408, 203, and 101 mAh g^{-1} at current densities of 100, 200, 500 – 5000 mA g^{-1}, respectively. Although the specific capacities of BM anode were higher than Mn_3O_4 in the first 20th cycle, the ones performed only under 10 mAh g^{-1} in the following cycles.

Figure 3c, d shows the cycling stability and capacity of BM and bulk Mn_3O_4 anodes in the voltage window of 0.01–3.00 V with the current density of 200 mA h g^{-1} for 50 cycles. For BM, specific capacities of the first charge and discharge cycle were approximately 526.9 and 525.3 mA h g^{-1} with an initial Columbia efficiency (CE) of 99.69%. Meanwhile, the first discharge/charge capacities of the Mn_3O_4 are 482.1/1310 mAh·g^{-1} with the first CE of 36.8%, illustrating and comparing to previous reports in Table 2. From cycles 2 to 50, the specific capacity of the battery decreased from 482.1 to 101 mAh g^{-1} with higher CE. It is common for previous studies to report a decrease in the capacity and stability of Mn_3O_4 materials used as a material for LIB anode [13-17].

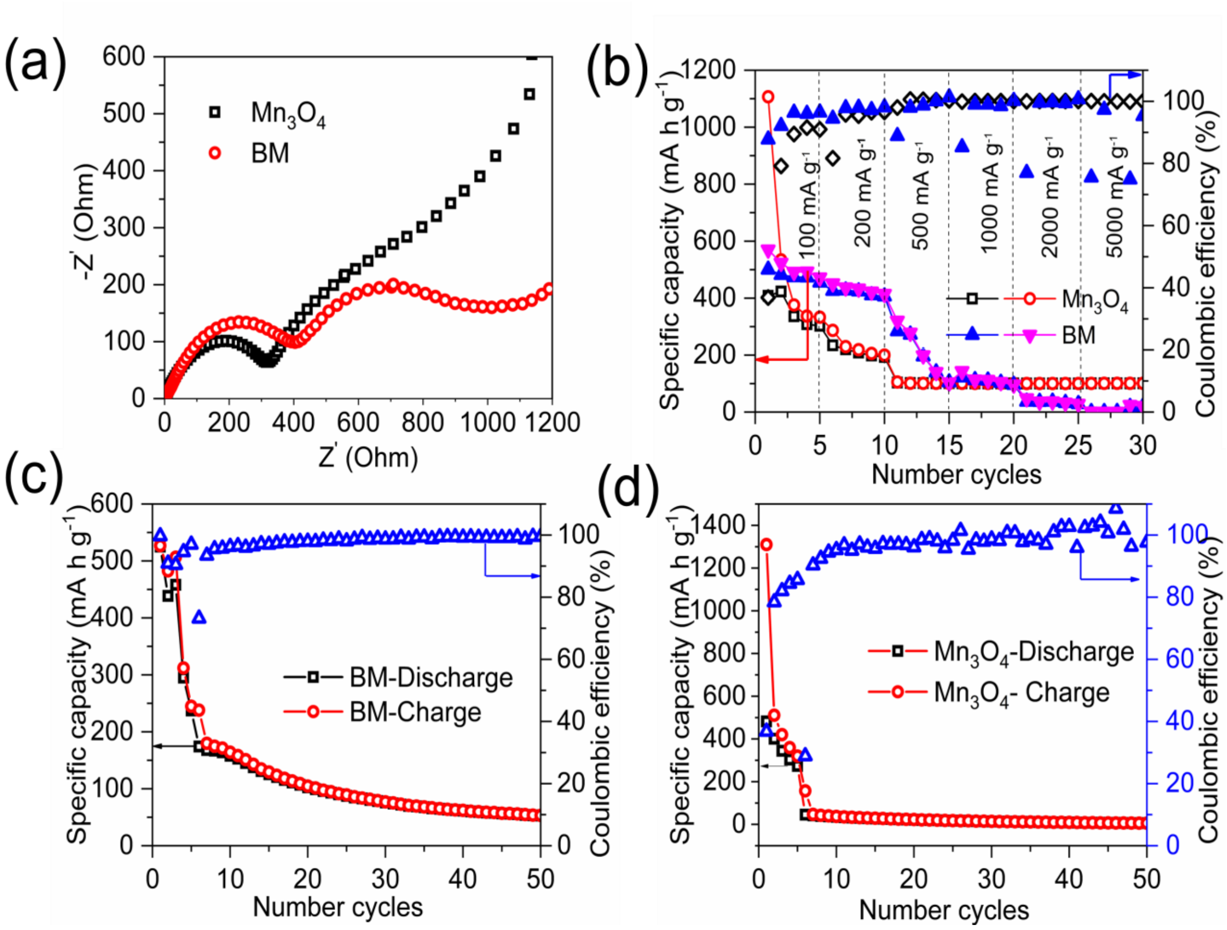

Fig 3. (a) - Nyquist plots, (b) - rate performance, (c, d) – Cycling of BM and Mn_3O_4 electrodes

Table 2. Comparison of the electrochemical performances of Mn_3O_4 anodes with the previous works

Sample	Initial Coulombic efficiency (%)	Initial discharge capacity (mAh g^{-1})	Discharge capacity after *n* cycles (mAh g^{-1})	Reference
Mn_3O_4 film	61.0	257	~100 (100 cycles)	[13]
Mn_3O_4 nanoparticles	60.4	290	190 (20 cycles)	[14]
Mn_3O_4 nanoparticles	32.0	522.3	~185 (100 cycles)	[15]
Mn_3O_4 nanoparticles	23.1	300	115 (only 10 cycless)	[16]
Mn_3O_4 microsphere	76.0	873	291 (only 10 cycles)	[17]
Mn_3O_4 nanoparticles	36.8	482	106 (50 cycles)	This work

Conclusion

In summary, the fabrication of hausmannite Mn_3O_4 nanoparticles has been reported by a simple thermal method at 550 °C under air using the black mass of spent primary batteries as a precursor. Electrochemical performances using cyclic voltammetry, galvanostatic charge-discharge, and EIS techniques were studied in detail on the electrodes as anodes for LIB. The results showed good electrochemical behavior of the Mn_3O_4 electrode with a specific discharge capacity of 102 mAh g^{-1} after 50 cycles and a good rate capacity of 208 mAh g^{-1} at a specific current of 1000 mA g^{-1}.

Acknowledgments

Le Thi Thanh Lieu was funded by the Postdoctoral Scholarship Programme of Vingroup Innovation Foundation (VINIF), code VINIF.2023.STS.22.

References

1. M. A. Salam, M. A. Gabal, and Y. M. Al Angari, J. Mater. Res. Technol., 18 (2022) 4267–4276. 2022. https://doi.org/10.1016/j.jmrt.2022.04.112
2. T. Skrzekut, A. Piotrowicz, P. Noga, M. Wędrychowicz, and A. W. Bydałek, Materials (Basel)., 15 (2022) 3966. https://doi.org/10.3390/ma15113966
3. S. Maryam Sadeghi, J. Jesus, and H. M. V. M. Soares, Waste Manag., 113 (2020) 342–350. https://doi.org/10.1016/j.wasman.2020.05.049
4. R. Farzana, M. A. Sayeed, J. Joseph, K. Ostrikov, A. P. O'Mullane, and V. Sahajwalla, ChemElectroChem, 7 (2020) 2073–2080. https://doi.org/10.1002/celc.202000422
5. B. Ebin, M. Petranikova, B. Steenari, and C. Ekberg, Waste Management & Research, 37 (2019) 168-175. https://doi.org/10.1177/0734242X18815966
6. Y. Selçuk, et al.,Batteries, 5 (2019) 35. https://doi.org/10.3390/batteries5010035
7. G. Belardi, R. Lavecchia, F. Medici, and L. Piga, Waste Manag., 32 (2012) 1945–1951. https://doi.org/10.1016/j.wasman.2012.05.008
8. L. Wang, L. Li, H. Wang, J. Yang, F. Wu, and R. Chen, ACS Appl. Energy Mater., 2 (2019) 23. https://doi.org/10.1021/acsaem.9b00839
9. M. Perachiselvi, M. S. Bagavathy, J. J. Samraj, E. Pushpalaksmi, and G. Annadurai, Appl. Ecol. Environ. Sci., 8 (2020) 273–277. https://doi.org/10.12691/aees-8-5-13
10. A. Vázquez-Olmos, R. Redón, G. Rodríguez-Gattorno, M.E. Mata-Zamora, F. Morales-Leal, A.L. Fernández-Osorio, J.M. Saniger, J. Colloid Interface Sci., 291 (2005) 175–180. https://doi.org/10.1016/j.jcis.2005.05.005
11. Y. Wang, C. Hou, X. Lin, H. Jiang, C. Zhang, and G. Liu, Appl. Phys. A Mater. Sci. Process., 127 (2021) 1–7. https://doi.org/10.1007/s00339-021-04428-6
12. T. Kozawa, F. Kitabayashi, K. Fukuyama, and M. Naito, Sci. Rep., 12 (2022) 1–12. https:// doi: 10.1038/s41598-022-16383-0
13. Y. Jiang, M. Hu, D. Zhang, and T. Yuan, Nano Energy, 5 (2014) 60–66. https://doi: 10.1016/j.nanoen.2014.02.002
14. Y. Wang, Journal of Materials Research, 3 (2015) 484-492. https://doi.org/10.1557/jmr.2014.394.
15. N. Fazila *et al.*, ACS Omega, 5 (2020) 29158–29167. https://doi.org/10.1021/acsomega.0c03888
16. H. Wang, L. Cui, Y. Yang, and H. S. Casalongue, J. Am. Chem. Soc., 132 (2010) 13978–13980. https://doi.org/10.1021/ja105296a
17. T. Kozawa, F. Kitabayashi, K. Fukuyama, and M. Naito, Sci. Rep., 11992 (2022) 12. https://doi.org/10.1038/s41598-022-16383-0